Table S1 Data collection and refinement statistics

	SP TACC3/CHC
Data collection	
Space group	$P6_1$ 22
Cell dimensions	
a, *b*, *c* (Å)	111.22, 111.22, 212.86
α, β, γ (°)	90.0, 90.0, 120.0
Resolution (Å)	2.15 (2.42-2.15) *
R_{pim}	0.017 (0.558)
$I / \sigma I$	23.0 (2.0)
Completeness (sphere %)	55.9 (9.4)
Completeness (ellipsoid %)	96.1 (87.1)
Redundancy	39.5 (38.9)
CC(1/2)	0.984 (0.785)
Refinement	
Resolution (Å)	96.33 – 2.15
No. reflections	24209
R_{work} / R_{free}	0.204/0.268
No. atoms	
Protein	4470
Peptide	159
Water	67
B-factors	
Protein	31.90
Peptide	37.93
Water	47.13
R.m.s. deviations	
Bond lengths (Å)	0.01
Bond angles (°)	2.28
Molprobity analysis	
Ramachandran outliers (%)	0
Ramachandran favored (%)	94.13
Clashscore	4.95
Molprobity score	2.04

*Values in parentheses are for highest-resolution shell.

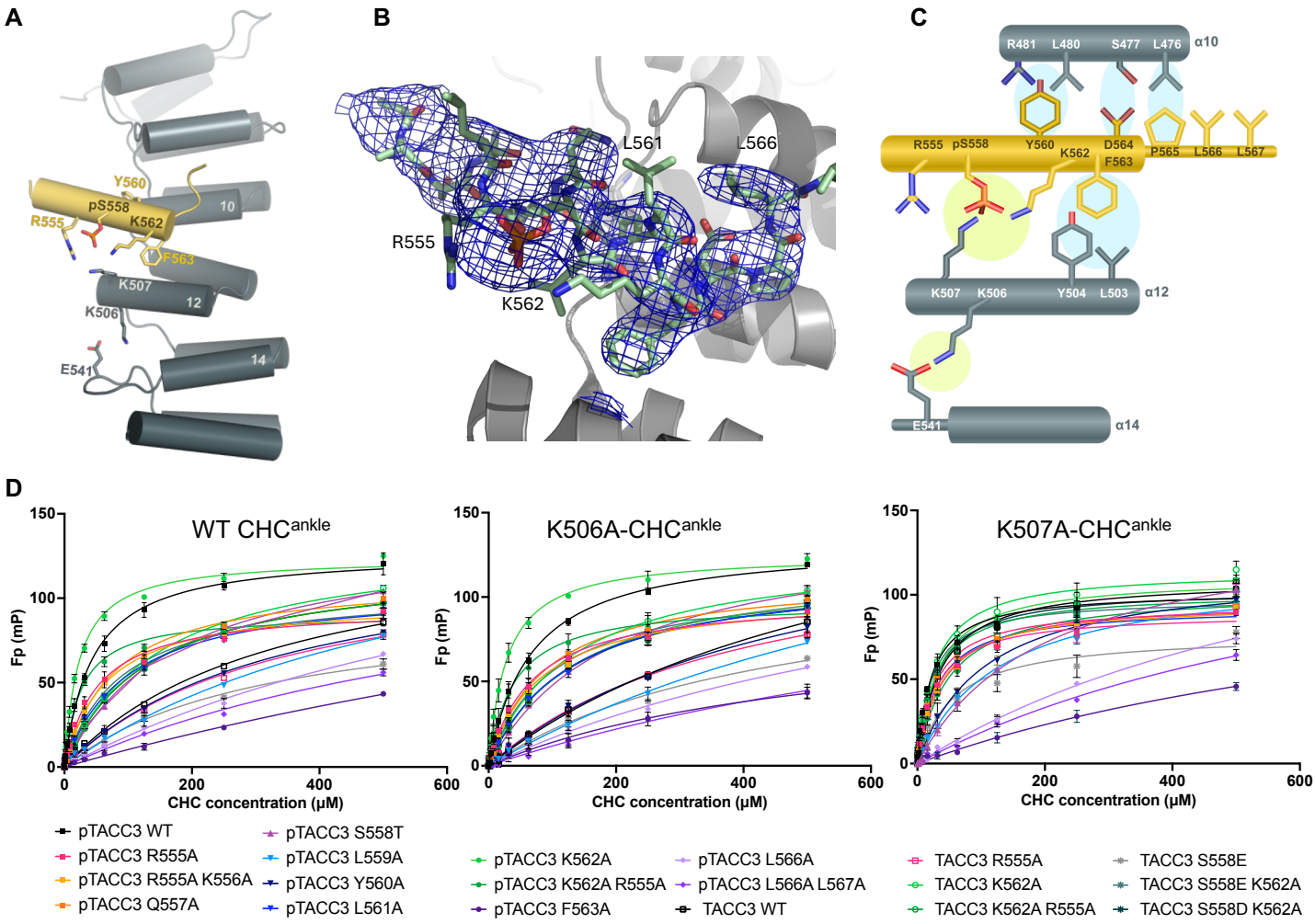

E

	CHC WT	CHC K506A	CHC K507A
pTACC3 WT	43 ± 4	66 ± 3	22 ± 5
pTACC3 R555A	52 ± 4	67 ± 3	29 ± 3
pTACC3 R555A K556A	64 ± 3	79 ± 2	37 ± 3
pTACC3 Q557A	78 ± 3	88 ± 3	28 ± 4
pTACC3 S558T	175 ± 2	201 ± 3	46 ± 3
pTACC3 L559A	605 ± 3	933 ± 3	129 ± 2
pTACC3 Y560A	350 ± 2	505 ± 3	107 ± 3
pTACC3 L561A	98 ± 3	127 ± 3	32 ± 3
pTACC3 K562A	23 ± 3	28 ± 4	32 ± 3
pTACC3 K562A R555A	26 ± 3	39 ± 5	50 ± 3
pTACC3 F563A	1912 ± 14	548 ± 3	959 ± 2
pTACC3 L566A	917 ± 2	859 ± 2	758 ± 2
pTACC3 L566A L567	793 ± 3	1186 ± 2	801 ± 3
TACC3 WT	335 ± 3	663 ± 3	36 ± 4
TACC3 R555A	340 ± 3	414 ± 3	40 ± 2
TACC3 K562A	146 ± 2	127 ± 3	28 ± 4
TACC3 K562A R555A	130 ± 2	136 ± 3	29 ± 4
TACC3 S558E	314 ± 3	459 ± 3	56 ± 6
TACC3 S558E K562A	88 ± 2	100 ± 3	22 ± 3
TACC3 S558D K562A	130 ± 2	130 ± 2	29 ± 3

Fig. S1: Hydrophobic and electrostatic interaction on CHC/pTACC3 binding interface. A Cartoon representation of the crystal structure of WT pTACC3 CID (aa 549-570) bound to the surface of CHC ankle domain (aa 358–574) [26]. **B** Fo-Fc electron density map contoured at 1.0 sigma around WT pTACC3 in the complex with CHC (PDB code 5ODS). Note clear density of pS558, F563, but poor density for R555, K562, L561 and ambiguous density for L566. **C** Schematic illustration of the CHC/pTACC3 interface with hydrophobic (blue) and electrostatic (yellow) interactions. **D** Direct binding fluorescent polarisation assays between FAM-labelled TACC3 and pTACC3 variant peptides (549–570) and WT CHC^{ankle} (left), K506A-CHC^{ankle} (centre) and K507A-CHC^{ankle} (right). **E** K_D values (μM) represent a mean of at least three experiments ± SD, values are colour-coded from the lowest K_D (dark grey) to the highest (yellow).

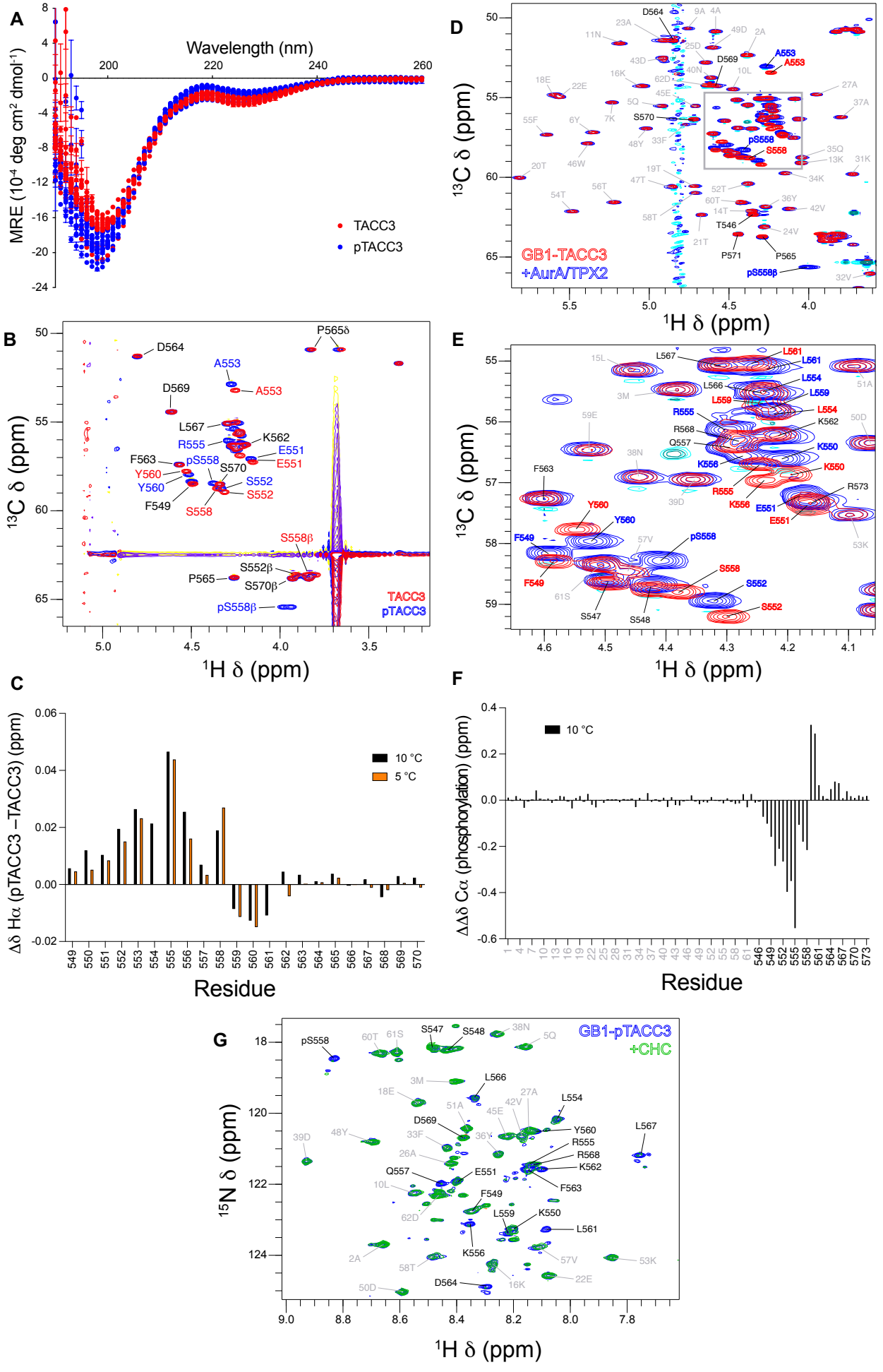
A
Wavelength (nm)
MRE (10⁴ deg cm² dmol⁻¹)
TACC3
pTACC3
B
¹H δ (ppm)
¹³C δ (ppm)
TACC3
pTACC3
C
Δδ Hα (pTACC3 –TACC3) (ppm)
10 °C
5 °C
Residue
D
GB1-TACC3
+AurA/TPX2
E
F
ΔΔδ Cα (phosphorylation) (ppm)
10 °C
Residue
G
GB1-pTACC3
+CHC
¹⁵N δ (ppm)

Fig. S2: Revised description of the structural changes within TACC3 upon phosphorylation of Ser558. A CD spectra for TACC3 (red) and pTACC3 (blue) peptides (50–80 μM) at 5 °C. Both peptides show a typical disordered profile. Based on the MRE value at 222 nm, estimates for the helicities of TACC3 and pTACC3 were 6 ± 1% and 5 ± 1%, respectively. **B** Cα region of $^{1}H–^{13}C$ HSQC spectra for TACC3 (red) and pTACC3 (blue) peptides (~0.8 mM) at 5 °C. The same result was found through *in situ* phosphorylation of TACC3 peptide with Aurora A. **C** Differences in Hα shifts for TACC3 and pTACC3 at 5 and 10 °C. The profile suggests a small, subtle shift in helical propensities across the peptide: residues prior to Ser558 have reduced propensity (+ve Hα changes) while Leu559, Tyr560 and Leu561 are increased (–ve Hα changes). **D** Cα region of $^{1}H–^{13}C$ HSQC spectra for a 140 μM $^{15}N/^{13}C$-labelled sample of GB1-TACC3 taken before (red) and after *in situ* phosphorylation with AurA–TPX2 (blue). Spectra were recorded at 10 °C (phosphorylation carried out at 20 °C). **E** Expansion of the congested region in the box in part D. **F** Differences in Cα secondary shifts upon phosphorylation of Ser558 in GB1-TACC3 with Aurora A (activated with TPX2). The Cα profile is clearer but mirrors that of the Hα changes in the peptide: residues prior to Ser558 have reduced propensity (–ve Cα changes) while later residues are increased (+ve changes). **G** $^{1}H–^{15}N$ HSQC spectra of *in situ* generated ^{15}N-labelled GB1-pTACC3 before (blue) and after (green) addition of CHC 1–574 (to 1:5 CHC:TACC3). Peak intensity loss mark the residues at or close to the binding site. Peaks with grey labels are from GB1. Spectra were recorded at 10 °C.

	K550	E551	S552	A553	L554	R555	K556	Q557	E558	L559	Y560	L561	K562	F563	D564	P565	L566	L567
WT	0.0	0.0	0.0	0.0	0.0	0.0	0.0	0.0	0.0	0.0	0.0	0.0	0.0	0.0	0.0	0.0	0.0	0.0
A	0.4	1.0	-0.3	0.0	1.2	0.8	-0.2	0.1	0.7	5.6	3.5	1.1	0.6	10.4	4.6	3.1	1.1	-0.9
G	0.0	3.0	1.7	2.7	4.3	3.6	3.6	3.7	3.8	9.9	8.2	4.0	4.6	16.5	8.9	6.5	0.5	-0.5
I	1.9	1.7	0.6	0.2	-0.1	0.2	-0.2	-1.5	0.1	0.3	-0.1	2.2	-2.0	8.1	5.4	2.4	8.0	0.5
L	1.2	0.6	0.4	0.0	0.0	0.3	-1.9	-1.3	0.1	0.0	-3.0	0.0	-3.3	5.9	2.5	3.9	0.0	0.0
P	-1.2	2.3	10.0	16.4	6.8	10.5	25.7	25.1	25.7	27.8	24.4	24.1	9.5	30.3	28.2	0.0	25.9	13.5
V	1.4	1.7	0.8	0.1	-0.1	0.0	0.2	-1.0	0.5	1.6	1.5	1.9	-1.8	7.1	2.0	2.6	8.8	0.3
F	0.2	1.7	1.8	-0.3	1.3	-1.4	-1.1	-0.6	0.7	3.2	-0.1	0.9	-0.6	0.0	4.9	1.1	-0.6	-0.2
W	0.0	1.5	1.3	-0.9	1.8	-2.5	-4.1	-1.4	-0.6	1.1	-1.0	-0.1	-1.1	9.5	7.2	3.8	-2.4	1.0
Y	0.3	1.4	1.2	-0.9	0.7	-0.9	-0.4	-2.1	0.2	1.9	0.0	0.6	-1.8	2.6	4.3	1.7	-0.5	-0.7
D	-0.3	-1.2	-1.6	-0.2	1.9	2.0	2.0	2.2	0.0	7.7	6.0	1.6	0.2	11.6	0.0	4.5	4.4	0.0
E	-0.5	0.0	-2.8	-0.4	1.5	0.6	0.6	0.7	0.0	5.5	3.8	2.2	0.3	12.1	3.1	3.7	4.2	-0.6
R	0.3	2.2	1.4	0.6	1.1	0.0	-0.3	-0.1	1.5	3.6	3.6	1.5	0.4	13.7	9.5	3.2	0.9	-1.3
H	0.0	1.6	1.5	0.6	0.2	0.8	0.7	0.0	1.3	4.7	3.6	1.9	-0.6	7.1	3.9	2.8	-1.3	-1.6
K	0.0	0.8	0.0	-0.4	0.0	0.7	0.0	-1.4	0.9	5.7	6.3	0.9	0.0	15.5	11.2	3.9	1.1	-0.8
S	-2.1	0.8	0.0	0.8	2.6	2.0	1.4	1.4	1.8	7.5	6.0	1.1	1.4	12.6	6.2	4.6	3.6	-1.3
T	-0.8	1.6	1.5	0.8	1.4	1.2	0.8	-0.3	0.9	3.8	3.6	2.1	-0.8	8.6	6.4	4.5	2.8	-0.9
C	2.6	3.6	2.5	1.9	3.8	3.3	2.1	2.0	2.7	6.6	4.0	2.7	2.1	9.0	4.5	4.9	0.3	-0.1
M	1.6	1.5	0.5	1.0	1.3	1.6	-1.9	0.1	1.5	0.6	1.0	1.0	-2.3	5.2	1.2	2.3	-1.6	-1.2
N	0.1	0.6	0.2	0.6	1.6	1.5	0.8	0.7	1.3	5.3	4.3	1.0	-0.1	9.8	2.5	4.4	-2.2	-1.6
Q	-0.1	1.4	0.1	0.8	1.4	0.7	0.2	0.0	0.6	4.3	4.1	1.3	-1.0	9.2	5.3	3.6	-4.3	-1.3

Fig. S3: Rosetta estimates of the effect of modified TACC3 sequences on affinity to CHC using *in silico* saturation mutagenesis based on the CHC/pTACC3 crystal structure model (PDB: 5ODS). A heatmap grid is used to represent the relative increase (red) or decrease (green) of total Rosetta energy compared to WT. For compatibility, pS558 was replaced with Glu. Rosetta was used to generate 50 relaxed structures of the 5ODS model (chains A and E). Using each of these 50 models as a starting structure, 20 new models for each mutation at each site as well as a WT repeat were generated using the cartesian-ddG application. The averaged total energy difference compared to the averaged WT value for each starting structure is shown in the grid. The outermost residues, although included in the calculations, are not coloured as they suffer from chain-end effects making them more permissive to mutation. As per the peptide array, Rosetta predicts substitutions Y560L and K562L to be most beneficial at these sites. Rosetta also shows the importance of retaining F563, D564 and P565 since all substitutions at the sites are destabilising. Suggested substitutions in the N-terminal half of the peptide (often to even more hydrophobic residues) were not considered further, although the flexibility in substitution of Q557 makes it appropriate for a stapling site.

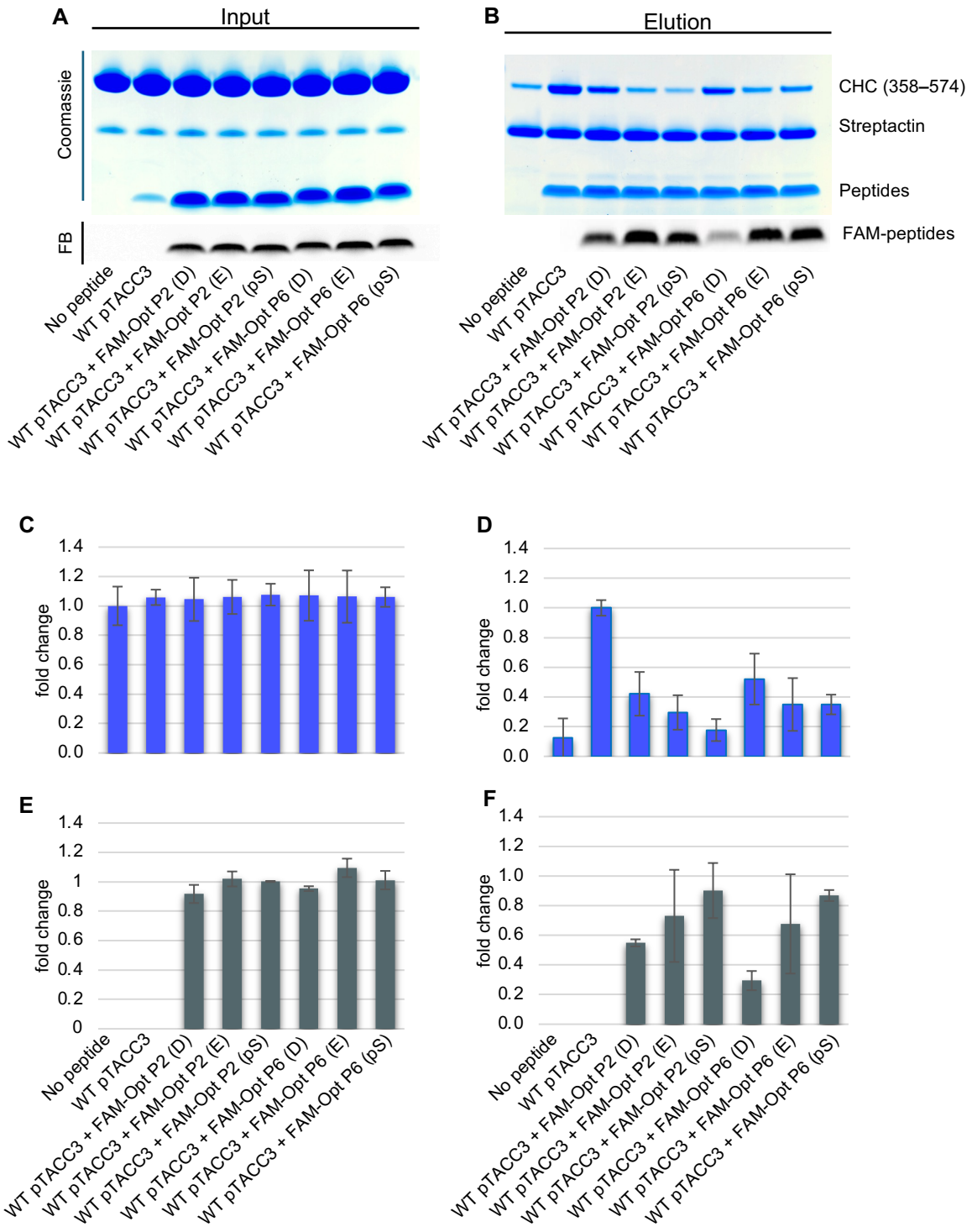

Fig. S4: Competition between sequence optimized TACC3 peptides and WT pTACC3 for binding to CHC (358–574). A Coomassie stained input and **B** elution of competitive pull-down assays of CHC with N-biotinyl-WT pTACC3 peptides immobilised on streptactin beads competing with FAM-Opt P2 and FAM-Opt P6 peptides containing pS/D/E substitution at the 558 position. FAM-Opt P2 and FAM-Opt P6 peptides in the assay were visualised on fluorescent blot (FB). A representative blot of an experiment performed in triplicates shown. **C** Quantification of CHC added to the pull-down reaction normalised to the control with N-biotinyl-WT pTACC3 only. **D** Quantification of CHC bound to N-biotinyl-WT pTACC3 in the elution of pull-down assays in the presence or absence of competing peptides FAM-Opt P2 and FAM-Opt P6, normalised to the N-biotinyl-WT pTACC3 control. **E** Quantification of FAM-Opt P2 and FAM-Opt P6 peptides added to the pull-down competition reaction and **F** bound to CHC in elution from the pull-downs, normalised to averaged fluorescence across input samples. Data in **C - F** represent the mean of three experiments; error bars indicate SD.

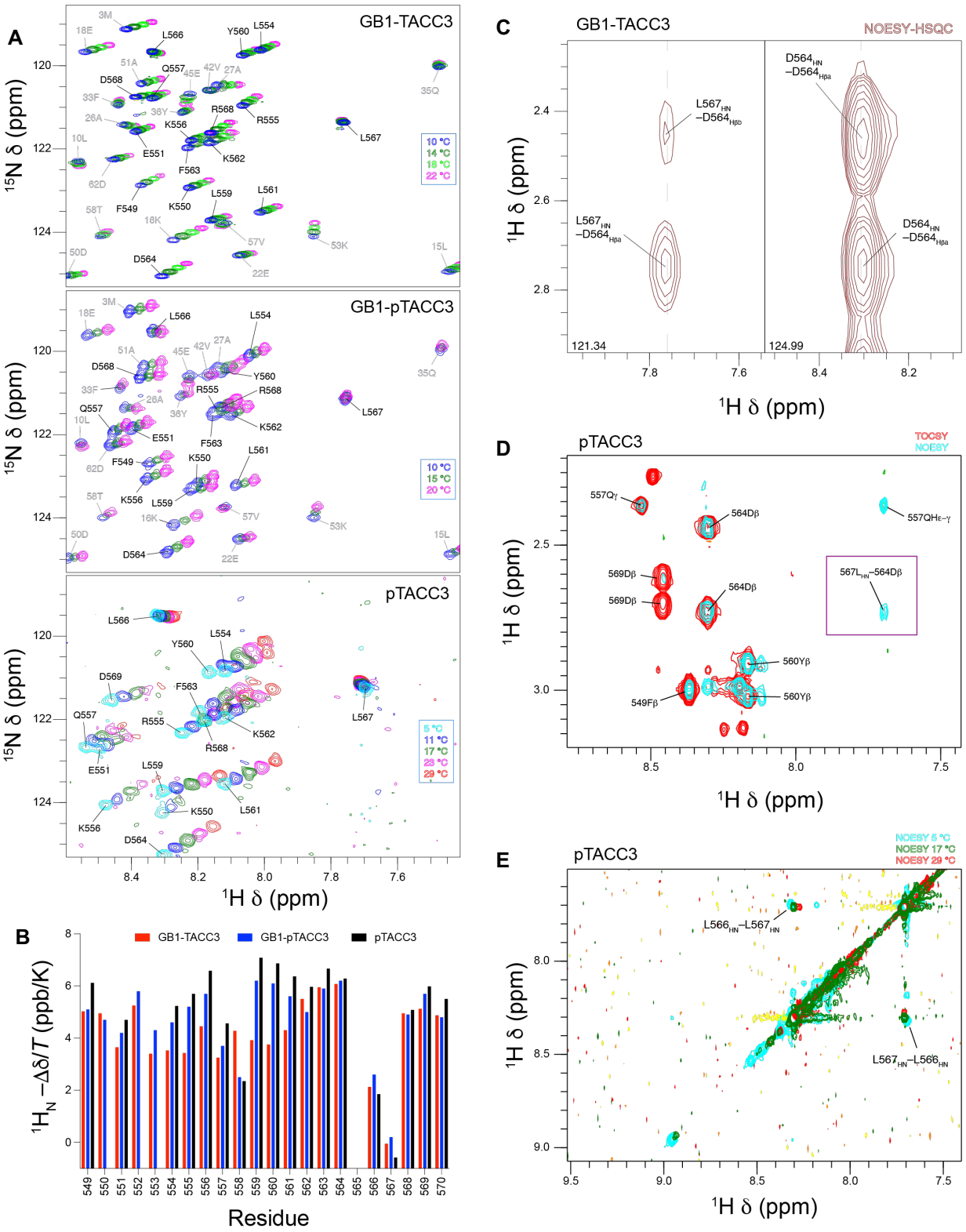

Fig. S5: A small structural motif in TACC3 exists prior to CHC binding. A ^{1}H–^{15}N correlation spectra (HSQC or HMQC) are shown for GB1-TACC3, GB1-pTACC3 and pTACC3. Except for L566 and L567, the ^{1}H–^{15}N peak positions for TACC3 residues tend to shift upfield in ^{1}H and ^{15}N on increasing temperature. Peaks with grey labels are from GB1. **B** Temperature coefficients for TACC3 $^{1}H_N$ nuclei from GB1-TACC3, GB1-pTACC3 and pTACC3 peptide data. **C** L567$_{HN}$–D564$_{Hβ}$ NOE cross peaks observed within a ^{1}H–^{15}N NOESY-HSQC spectrum of GB1-TACC3 at 10 °C and **D** a ^{1}H–^{1}H NOESY spectrum of pTACC3 peptide at 5 °C (^{1}H–^{1}H TOCSY included for comparison). Note also the large difference in shifts for the two 564 Hb protons (*cf.* those for D569) local structure being a means to strongly differentiate the two environments. **E** HN–HN cross peaks between L566 and L567 in pTACC3 peptide over a range in temperature.

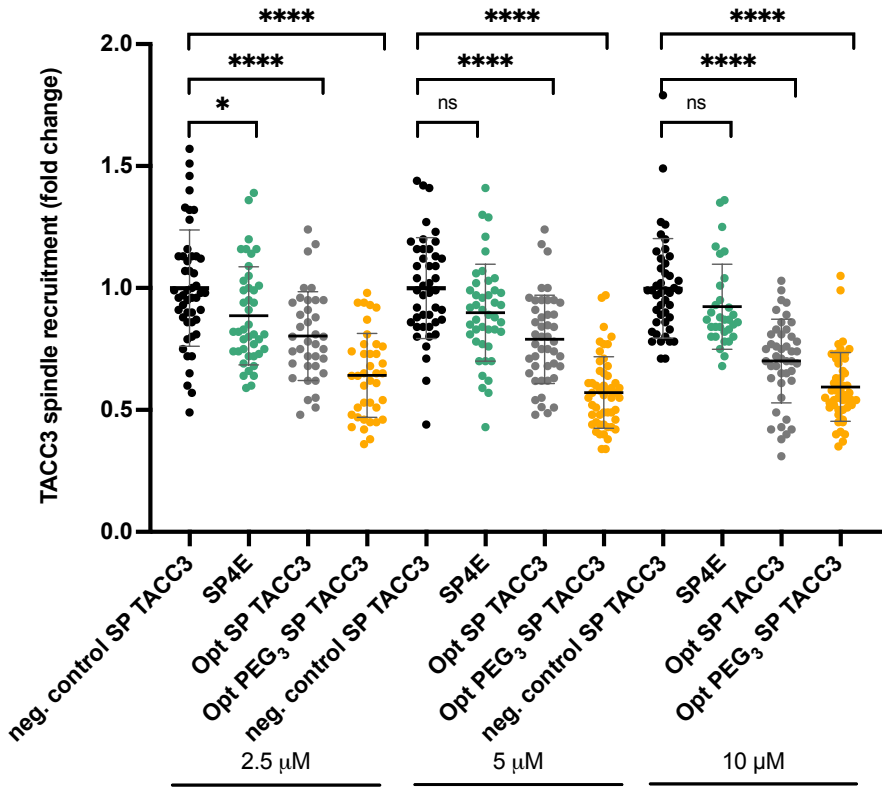

Fig. S6: Quantification of endogenous TACC3 localization on mitotic spindles of HeLa cells in metaphase. Cells were treated with 2.5, 5 and 10 μM FAM-TACC3 peptides. Each circle represents a single cell, n=32-51 cells per each peptide concentration measurement pooled from three independent experiments. The measurements were normalised to the average negative control fluorescence value. The short bar and error bars show the mean ± SD, respectively. ANOVA with Tukey's post-hoc test was used to compare the means between each group. The *p*-value is shown compared to the negative control SP TACC3 peptide: **** $p<0.0001$; * $p<0.05$; ns $p>0.05$.

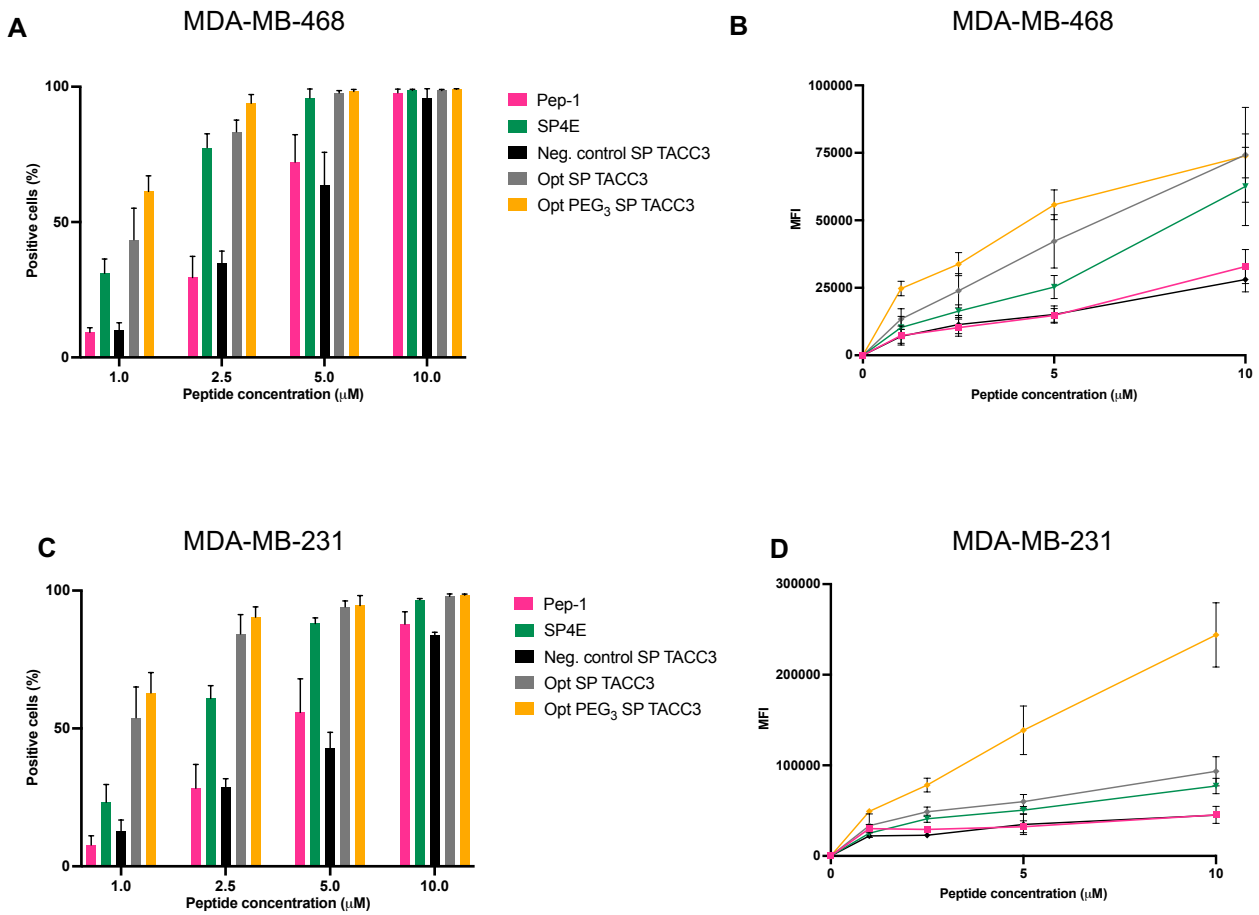

Fig. S7: Uptake of FAM-conjugated stapled TACC3 peptides by MDA-MB-468 and MDA-MB-231 breast cancer cell lines. Cells were treated with increasing concentration of the peptides (1-10 μM) for 60 min before measurement by flow cytometry **A, C** The ratio of MDA-MB-468 and MDA-MB-231 cell, respectively, containing internalised peptides (%). **B, D** Mean fluorescence intensity (MFI) in the breast cancer cell lines measurements show a dose-dependent increase in cell internalization. Error bars represent the SD of three biological replicates.

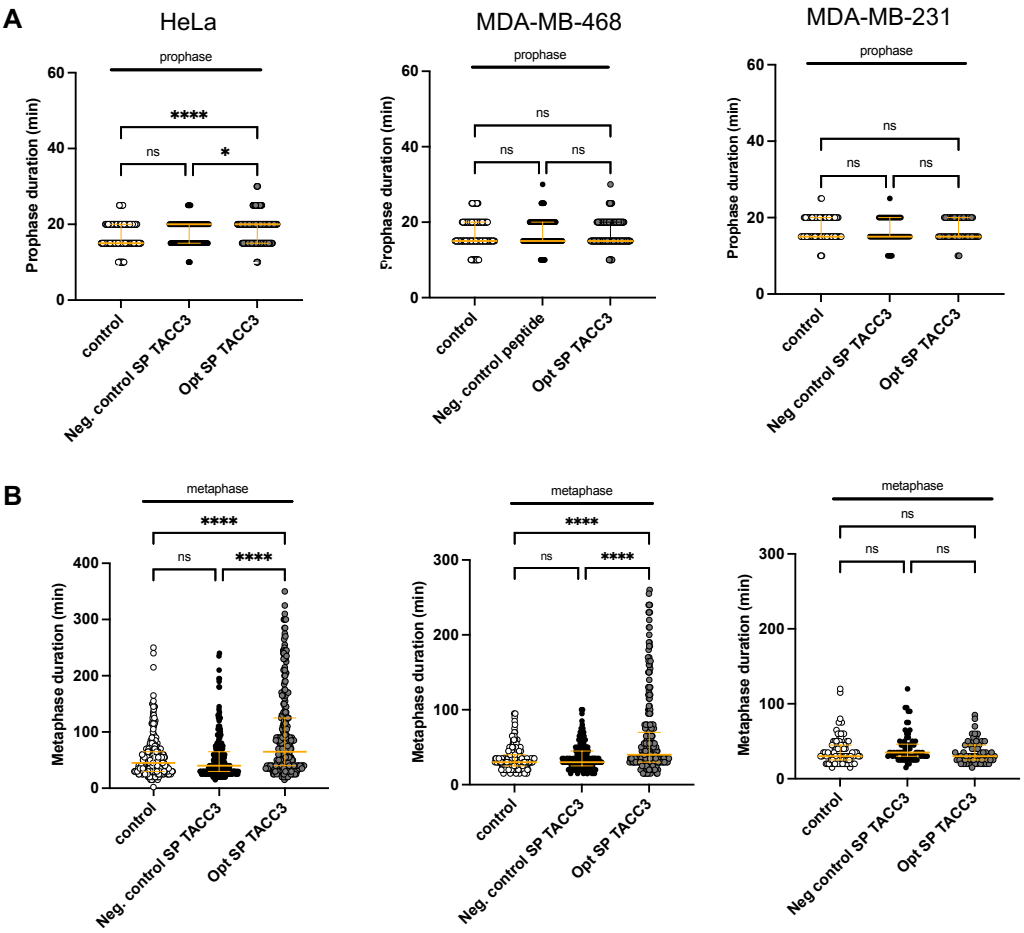

Fig. S8: Treatment of cells with stapled peptides results in a slower progression through mitosis, affecting predominantly metaphase duration. Scatter plot of the time in mitosis showing the stapled peptide treatment affecting predominantly the length of time cells spend in metaphase. **A** The length of prophase is defined from NEBD to fully established mitotic spindle in SiR-tubulin-labelled HeLa cells, MDA-MB-468 and MDA-MB-231 cells treated with 5 µM neg. control SP TACC3, SP TACC3 and untreated control; each dot represents a single cell (mitotic event count identical to Fig. 7) Data were collected for 10 h, with data acquisition every 5 min; **B** Scatter plot of the length of metaphase until anaphase onset measured in the identical set of cell lines under the conditions described in Fig 7. The plots indicate the median and interquartile ranges (25th–75th percentile). Kruskal-Wallis test results show the *p*-value: **** $p<0.0001$, * $p<0.05$, ns $p>0.05$.

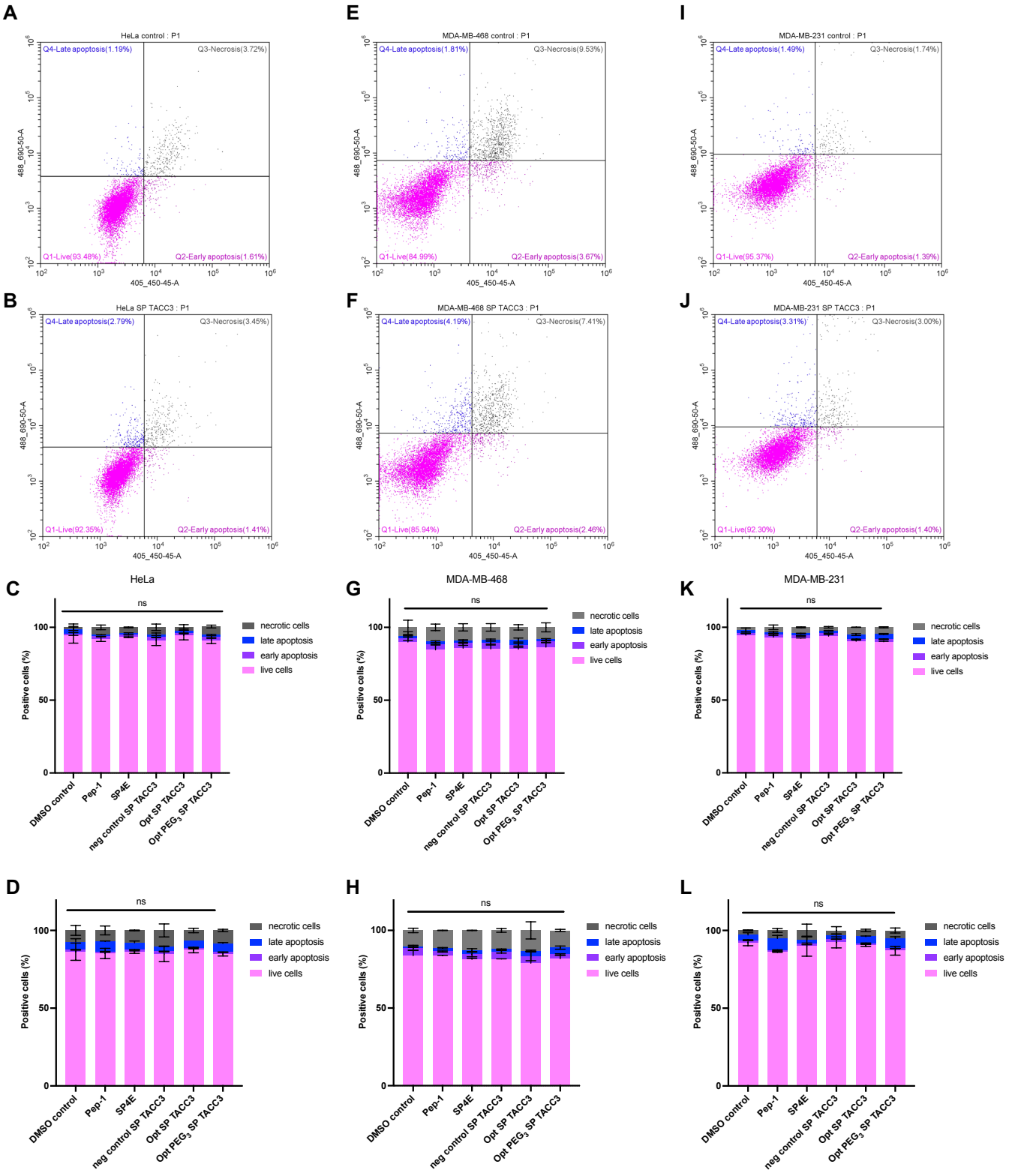

Fig. S9: Cell viability assays show no cytotoxic effects following treatment with stapled peptides. **A** Representative images of cell viability measurements of DMSO control and **B** Opt SP TACC3 peptide-treated HeLa cells measured by flow cytometry using Pacific Blue-Annexin V and PI staining. **C** Quantification of cytometry assays of HeLa cells treated for 24 h with 5 µM peptides and **D** 10 µM peptides. **E** Representative images of cell viability measurements of DMSO control and **F** Opt SP TACC3 peptide-treated MDA-MB-468 cells stained with Pacific Blue-Annexin V and PI. **G** Quantification of cytometry assays of MDA-MB-468 cells treated for 24 h with 5 µM peptides and **H** 10 µM peptides. **I** Representative images of cell viability measurements of DMSO control and **J** Opt SP TACC3 peptide treated MDA-MB-231. **K** Quantification of cytometry assays of MDA-MB-231 cells treated 24 h with 5 µM peptides and **L** 10 µM peptides. Data represent the mean of two experiments; error bars indicate SD. ANOVA with Tukey's post-hoc test was used to compare the means between each group. The *p*-value: ns $p>0.05$

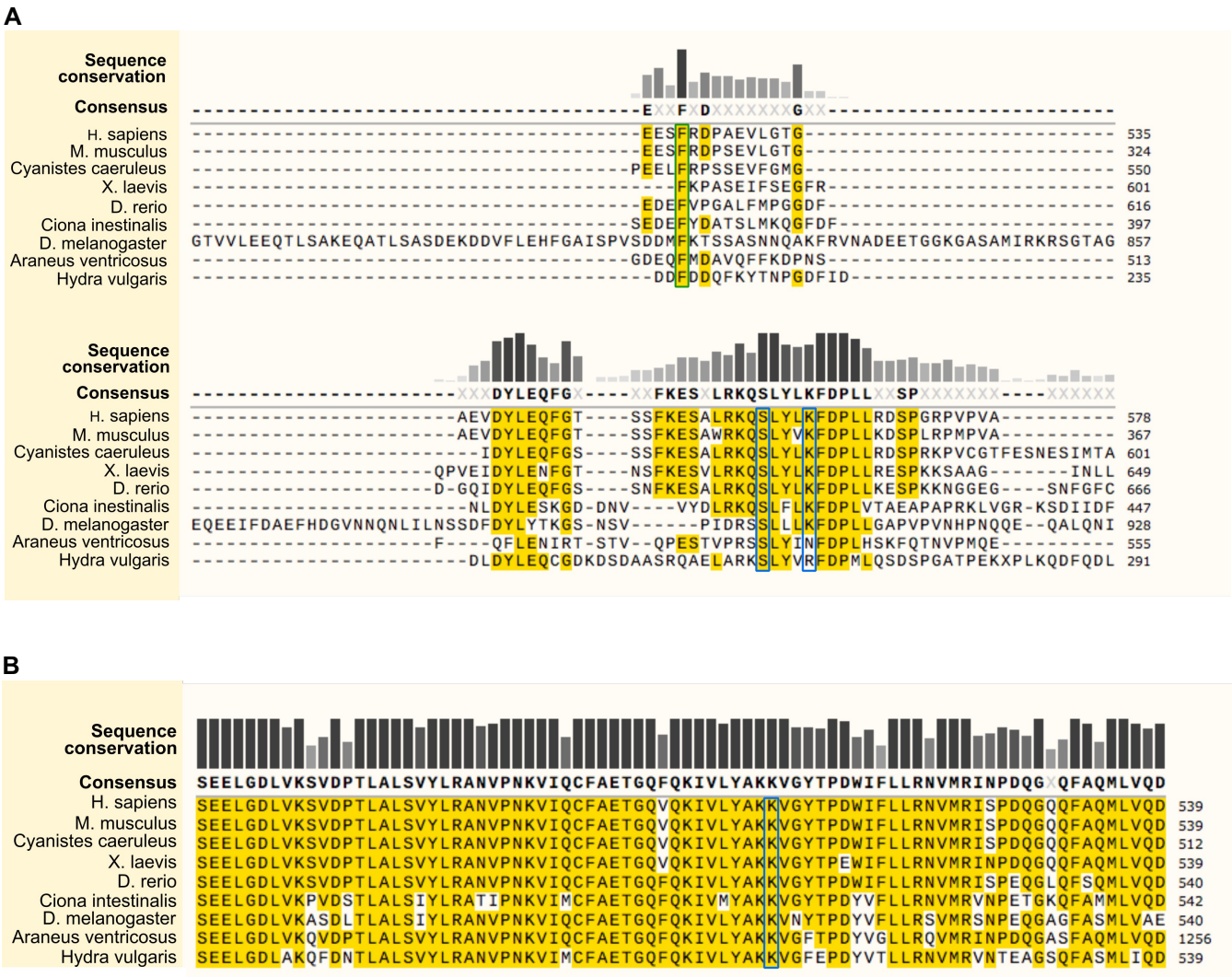

Fig. S10: Sequence alignment of the CHC/TACC3 interface. **A** Multiple sequence alignment of TACC3 and **B** clathrin heavy chain orthologs spanning the regions involved in the interface. The conserved residues are highlighted in yellow. Key binding residues (S558^{TACC3}, K562^{TACC3} and K507^{CHC} are boxed in blue. The F525^{TACC3} residue required for binding to Aurora A is boxed in green.